A robust, highly reversible, mixed conducting sodium metal anode

Keshuang Cao¹, Qianli Ma^{2,*}, Frank Tietz², Ben Bin Xu³, Mi Yan¹, Yinzhu Jiang^{1,*}

¹School of Materials Science and Engineering, State Key Laboratory of Clean Energy

Ultilization, Zhejiang University, Hangzhou 310027, China

²Forschungszentrum Jülich GmbH, Institute of Energy and Climate Research, Materials

Synthesis and Processing (IEK-1), 52425 Jülich, Germany

³Smart Materials and Surfaces Lab, Mechanical Engineering, Faculty of Engineering and

Environment, Northumbria University, Newcastle upon Tyne NE1 8ST, UK

Email: q.ma@fz-juelich.de (Q. Ma); yzjiang@zju.edu.cn (Y. Jiang),

abstract: Sodium metal anode holds great promise in pursuing high-energy and sustainable rechargeable batteries, but severely suffers from fatal dendrite growth accompanied with huge volume change. Herein, a robust mixed conducting sodium metal anode is designed through incorporating NaSICON-type solid Na-ion conductor into bulk Na. A fast and continuous pathway for simultaneous transportation of electrons and Na⁺ is established throughout the composite anode. The intimate contact between Na-ion conducting phase and Na metallic phase constructs abundant two-phase boundaries for fast redox reactions. Further, the compact configuration of the composite anode substantially protects Na metal from being corroded by liquid organic electrolyte for the minimization of side reactions. Benefiting from the unique configuration, the composite anode shows highly reversible and durable Na plating/stripping behavior. The symmetric cells exhibit ultralong lifespan for over 700 h at 1 mA cm⁻² with a high capacity of 5 mAh cm⁻² and outstanding rate capability up to 8 mA cm⁻² in the carbonate

electrolyte. Full cells with Na₃V₂(PO₄)₃/C cathode demonstrate impressive cycling stability (capacity decay of 0.012% per cycle) and low charge/discharge polarization as well. This work provides new insights into rational design and development of robust sodium metal anode through an architecture engineering strategy for advanced rechargeable sodium batteries.

Keywords: Sodium metal battery; Sodium metal anode; Solid Na-ion conductor; Dendrite; Cycling stability

1. Introduction

Rechargeable lithium-ion batteries (LIBs) have tremendously powered our daily life ranging from portable electronics, electric vehicles to energy storage systems [1-3]. Given the overwhelming benefits it brought to humanity, the Nobel Prize in Chemistry rewarded its pioneers in 2019. However, the scarcity and uneven distribution of lithium resources [4-7] have always been a dark cloud over LIBs, akin to the well-known "oil shocks". With the rapidly growing demand for energy storage, such concerns become even more serious. From this perspective, alternative energy storage techniques are urgently needed [8], where sodium-based batteries have shown great competitiveness due to the abundance of sodium resources and the similar electrochemical working principle to that of LIBs [9-12]. Among sodium-based batteries, difficulties are encountered in the exploration of appropriate anodes, wherethe conventional graphite anodes in LIBs have failed to succeed toward sodium storage [13, 14]. Like Li-metal anode in lithium metal batteries, there have been emerging interests in Na- metal anode for high-energy rechargeable metal batteries, owing to its highest theoretical capacity (1165 mAh g-1) and lowest electrochemical potential (-2.71 V vs. standard hydrogenelectrode) in sodium-based systems [15, 16]. Unfortunately, Na-metal anode suffers from a

series of problems such as huge volume change during cycling, unstable and fragile solid electrolyte interphase (SEI) and uncontrollable dendritic growth, which is extremely seriousin carbonate electrolytes, aggravates the safety concerns and hinder its practical application [17-19].

There have been numerous efforts devoting to stabilizing Na-metal anode through replacing the intrinsic unstable SEI layer by building spontaneously or artificially a robust protectionone [20-22], resulting in stable plating/stripping process and prolonged cycling stability. However, the relatively sluggish Na⁺ diffusion compared to the fast electron transport in bulk Na-metal will concentrate Na plating/stripping on the two-dimensional planar surface of Na- metal, not into the depth of electrode, which inevitably induce the severe deformation of electrode under moderate current density and areal capacity (1 mA cm⁻² and 1 mAh cm⁻²). It should be noted that an electrode areal capacity of at least 3 mAh cm⁻² is needed for actual battery operation [19]. To fulfill the requirement, 3D current collectors, such as 3D porous Cu[23, 24], functional carbon materials [25-27] and Mxenes [28], were utilized to accommodate volume fluctuation of Na and reduce local current density to stabilize Na-metal anodes. Whereas these modified current collectors generally possess high specific surface area, which will expose more Na metal directly to the liquid organic electrolyte, they further exacerbate the side reactions in the initial stage [29]. Moreover, as the plating/stripping of Na still occurs on the surface of the electrode, the problems caused by the intrinsic fragile and heterogeneous SEI have not been resolved. In consideration of the sluggish Na⁺ diffusion in Na-metal, the integration of an ion-conducting network into bulk Na-metal is critical for plating/stripping of Na in the whole electrode volume. Therefore, a robust hybrid design of bulk electrode might include: (1) fast/balanced mixed electron/ion conducting pathways; (2) abundant interfacial area in the whole electrode volume for Na plating/stripping; (3) minimization of liquidorganic electrolyte exposure; (4) rigid skeleton to accommodate volume fluctuations of Na;

(5) facile and scalable process for bulk hybrid electrode.

Herein, a dendritic-free and stable bulk hybrid Na-metal anode (BH-Na) has been demonstrated through incorporating NaSICON-type solid electrolyte into bulk Na as 3D ion- conducting pathways (Fig. 1a). Owing to the rich and intimate contact between Na metal and solid electrolyte, abundant two-phase boundaries in the whole electrode volume are formed for stable Na plating/stripping benefitting from the balanced Na ion and electron flux (Fig. 1b). Furthermore, the rigid solid electrolyte network and the compact configuration of the bulk hybrid anode effectively minimize the direct exposure to liquid organic electrolyte, accommodate the volume variation of electrode, and the enhanced mechanical strength inhibits the growth of Na dendrites. High rate capability, low polarization and ultralong cycling lifespan are simultaneously achieved in both symmetrical cells and full cells based on the hybrid design of bulk electrode.

2. Experimental

2.1. Fabrication of SnO₂@NZSP

Na_{3.4}Zr₂Si_{2.4}P_{0.6}O₁₂ (NZSP) was synthesized by a solution-assisted solid-state reaction method reported by Ma et al. [30]. Typically, NaNO₃ and ZrO(NO₃)₂ were dissolved into distilled water, then Si(OCH₂CH₃)₄ and NH₄H₂PO₄ were sequentially added to the solution while stirring. The dosage of reagents is strictly in accordance with the stoichiometric ratio. The solution then becomes a mixture of colloidal sol and precipitates of zirconyl oxyphosphate compounds. After drying at 85 °C, the obtained powder was calcined at 1100 °C for 3 h to obtain NZSP powder. Afterwards, SnCl₂ was dissolved in *N*,*N*- dimethylformamide (DMF) to prepare a solution with 0.5 mol L⁻¹. Then NZSP powder was added and the mass of SnCl₂ in the solution was controlled to be 15% of the mass of NZSP. After stirring for 2 h, the solution was dried overnight in an oven at 80 °C. Subsequently, the powder was ground and then sintered at 450 °C for 2 h in air to obtain the SnO₂@NZSP powder.

2.2. Fabrication of BH-Na anode

Melt infusion method was conducted in an argon-filled glove box ($O_2 \le 0.1$ ppm, $H_2O \le 0.1$ ppm). $SnO_2@NZSP$ powder and fresh Na metal of equal mass were put into a Nickel crucible and heated to 250 °C. After stirring for about 5 min, molten sodium was completely immersed in the $SnO_2@NZSP$ powder, and they were mixed together like a semi-solid slurry exhibiting metallic luster. Then the mixture was cooled down and after mechanically pressing, it was punched into a disc with a diameter of 1.2 cm and a mass of ~ 0.064 g, and was applied as the BH-Na anode.

2.3. Fabrication of Na₃V₂(PO₄)₃/C cathode

Porous carbon-coated Na₃V₂(PO₄)₃ cathode was prepared by the same process as reported earlier [31]. NH₄VO₃ was dissolved in distilled water at 80 °C, then H₄H₂PO₄ and NaOH were added with stirring. After that, citric acid was added as both a carbon source and a reducing agent, which had the same molar concentration as the vanadium source in the solution. The dosage of reagents is strictly in accordance with the stoichiometric ratio. After stirring for 2 h, the solution was evaporated overnight at 80 °C in an oven. Then, the dried product was ground and annealing at 800 °C for 10 h under an argon atmosphere. Finally, Na₃V₂(PO₄)₃/C cathode was obtained.

2.4. Materials characterization

The mass ratio of Sn was measured by inductively coupled plasma-optical emission spectrometry (ICP-OES, Agilent 720ES). To calculate the ionic conductivity of NZSP, the impedance spectra of sintered NZSP pellet (with gold blocking electrodes) was examined by Novocontrol Alpha-A electrochemical systems, with an AC frequency range from 10 MHz to 100 Hz. The morphology of samples was characterized by scanning electron microscopy (SEM, HITACHI SU8010). For preparing the SEM samples of electrodes in different Na plating/stripping states, an additional Celgard 2300 microporous polypropylene separator was placed on each side of the glass fiber separator during battery assembly to prevent the glass

fiber separator affecting the observation of the morphology. The electrodes after cycling were

taken out from the disassembled cell, then they were rinsed with diethyl carbonate (DEC) to remove the electrolyte. Afterwards the samples were affixed to the SEM stage by conductive adhesive and transferred carefully into the electron microscope minimizing the exposure of samples to the atmosphere. The sample preparations were performed in an Ar-filled glovebox and the SEM stage was transferred with an airtight holder. X-ray diffraction (XRD) patterns were performed on an X-ray diffractometer (Bruker D8 Advance, Germany) with Co K α radiation (λ = 1.7902 Å) at 35 kV, 28 mA. Samples containing metallic sodium were covered with Kapton tape to prevent the sodium metal from reacting with air.

2.5. Electrochemical measurements

For electrochemical investigations, CR2025 coin cells were assembled in an argon-filled glovebox. A commonly used carbonate-based electrolyte 1 mol L⁻¹ NaPF₆ in ethylene carbonate/diethyl carbonate/propylene carbonate (EC/DEC/PC, 4:4:2, volume ratio) with the addition of 5% fluoroethylene carbonate (FEC) was used in all the tests. The symmetric cells were assembled with two identical electrodes. In the typical battery assembly process, a Whatman glass fiber membrane served as the separator. Electrochemical impedance spectroscopy (EIS) and Tafel plot of the symmetrical cell after 10 cycles at 1 mA cm⁻² and 1 mAh cm⁻² were conducted by a CHI660C electrochemical workstation. Specifically, EIS was examined in the frequency range from 1 MHz to 1 mHz with an amplitude of 5 mV, the scan rate of Tafel plot tests was 10 mV s⁻¹. For full cells, Na₃V₂(PO₄)₃/C, Super P and PVDF in theweight ratio of 8:1:1 in NMP solvent were mixed. After the slurry was uniformly coated on the carbon-coated Al foils via doctor blading, the electrodes were dried in a vacuum drying oven at 110 °C overnight. The mass load of electrodes was about 1 mg cm⁻².

3. Results and discussion

 $Na_{3.4}Zr_2Si_{2.4}P_{0.6}O_{12}$ (NZSP), a typical NaSICON solid electrolyte, exhibits one of thehighest sodium conductivity among all oxide-based Na-ion conductors, which is about 4.8 \times 10^{-3} S cm⁻¹ at 25 °C (Fig. S1a online) and comparable to that of liquid organic electrolyte

[30]. Hybrid design of bulk Na-metal-based electrode was designed through a facile melt infusion strategy in which molten Na was mixed with surface-modified NZSP particles. In a typical process, a conformal SnO2 layer was pre-coated on the surface of NZSP particles for better affinity with molten Na, in which SnO₂ can reacts with Na to form Na-Sn alloy under heating to significantly improve the wettability of Na. As shown in Figs. 1c and S1b (online), no obvious change is found in the morphology for SnO₂-coated NZSP particles. The homogeneous distribution of Sn in EDS mapping (Fig. 1d) and the existence of crystalline SnO₂ phase (Fig. 1e) clearly verify the uniform coating of SnO₂ on the NZSP particles. The mass fraction of the SnO₂ coating layer in SnO₂@NZSP is about 8.62 wt% as determined by the ICP-OES measurement. Afterwards, the molten Na was mixed with modified NZSP in an optimal mass ratio of 1:1 for constructing the BH-Na electrode (Fig. 1a). In contrast, unmodified NZSP particles exhibit poor wettability against molten Na (Fig. S2 online). The as-obtained BH-Na electrode shows a compact microstructure with homogeneous distribution of NZSP and Na as shown in Figs. 1f and S3 (online). Moreover, besides the expected reflections of NZSP, Na₁₅Sn₄ and Na, no other reflections are detected in the XRD pattern of the BH-Na electrode (Fig. S4 online), confirming the good chemical stability between modified NZSP and Na. Furthermore, the BH-Na electrode demonstrates about twofold higher hardness as compared to the bare Na-metal (Figs. 1h and S5 (online)), which is beneficial for inhibiting dendritic growth due to the enhanced mechanic strength [32]. Such hybrid electrode delivers a close-to-the-theoretical capacity of 1150 mAh g ¹ based on the mass of Na-metal (Fig. S6 online), implying that almost all of the sodium can be stripped out while the solid electrolyte network remains stable (Fig. 1g).

Symmetric cells were assembled with 1 mol L⁻¹ NaPF₆ in carbonate electrolyte to investigate the Na plating/stripping behavior of BH-Na electrode as shown in Fig. 2. It is widely known that stable plating/stripping of Na is extremely difficult with conventional carbonate electrolyte due to its high corrosivity to Na metal [33-35]. This perspective is

verified with bare Na-metal which shows dramatic fluctuations in voltage profile, which lasts for only 89 h till the occurrence of short-circuiting. On the contrary, the BH-Na electrode exhibits a stable plating/stripping process for over 750 h at 1 mA cm⁻² with a capacity of 1 mAh cm⁻² (Fig. 2a). More details in plating/stripping process can be obtained from the enlarged voltage profiles during the different periods of cycling, as shown in the insert of Fig. 2a. Dramatic overpotential peaks at the beginning and end of the charge/discharge curves are observed for the bare Na-metal symmetric cell, which can be ascribed to the dendrite growth and the formation of pits during Na plating/stripping [29, 36]. In contrast, except for the initial cycles of activation process, the BH-Na electrode presents a flat voltage curve with ultra-low overpotential (~35 mV), indicating uniform plating/stripping behavior with low energy barrier, which might be ascribed to the improved Na⁺ transport resulted from the 3D Na-ion conducting network in the BH-Na electrode. The effects of different proportions of NZSP on electrochemical performance were also investigated as shown in Fig. S7 (online). As expected, the electrodes with higher NZSP content were able to perform faster and stable Na plating/stripping due to richer two-phase boundaries and denser ion conduction networks.

The role of the NZSP skeleton is further confirmed by EIS (Fig. 2b) and Tafel plots (Fig. 2c). After 10 cycles, the BH-Na electrode delivers a much lower charge transfer resistance (\sim 12 Ω), which is only one-tenth the value of the bare Na electrode (\sim 126 Ω), suggesting much enhanced electrochemical kinetics of BH-Na. According to the Tafel plots, the BH-Na electrode exhibits two-fold higher more exchange current density than that of the bare Na electrode (0.52 vs. 0.15 mA cm⁻²). The higher exchange current density means the lower energy barrier that the Na⁺ must overcome moving from the electrolyte to the reaction area [37]. Accordingly, the redox reactions in the BH-Na electrode will be more easily to occur. For further verification of the role of the NZSP ion-conducting network, control experiments were conducted using Na ion-insulating ZrO₂ particles to fabricate the hybrid anode.

Specifically, ZrO₂ with average particle size similar to NZSP (~200 nm) was selected to

prepare the ZrO₂-Na anode, and considering the difference in density between ZrO₂ and NZSP, two groups of ZrO₂-Na anodes with the same volume fraction and the same mass ratio as the optimal BH-Na anode were prepared for the test. Figs. S8 and S9 (online) reveal that the increase in mechanical strength can improve the stability of the composite anode to a certain extent. However, compared to the BH-Na anode, the ZrO₂-Na anode delivers larger polarization, higher charge transfer resistance, as well as shorter lifespan, whether the same mass ratio or volume fraction of particles is applied to the ZrO₂-Na anode. These results imply that the fast ion transport of the NZSP skeleton is crucial for improving the electrochemical performance of the hybrid anode.

To meet the more stringent requirements in practice, a higher current density along with a higher capacity was employed in the assessment of symmetric cells. At a practical Na deposition capacity of 5 mAh cm⁻² with 1 mA cm⁻² (Fig. 3a), the cell with the BH-Na electrode exhibits a low overpotential of 36 mV and flat voltage plateau for over 700 h. It is worth noting that such an ultralong lifespan has never been achieved under the same test condition in conventional carbonate electrolyte (Table S1 online). However, the overpotential of the bare Na cell is large and fluctuates sharply, resulting in a soft short-circuit after 26 h. When the current density was increased to 3 mA cm⁻² with a fixed capacity of 3 mAh cm⁻² (Fig. 3b), the BH-Na electrode still maintains stable for over 150 h with a small overpotential.Instead, for the bare Na electrode, the short-circuiting occurs only after 27 h. In addition, the BH-Na electrode also exhibits remarkable rate capability at stepwise increased current densities up to 8 mA cm⁻² (Fig. 3c). Low overpotential of 34, 47, 114, and 210 mV are obtained for the BH-Na electrode at current density of 1, 2, 5, and 8 mA cm⁻², respectively, much lower than those of the bare Na electrode (170, 216, 294, and 376 mV).

The above results have clearly revealed that the introduction of 3D continuous and fast ion pathways along with the compact configuration of electrode can significantly reduce the polarization and improve the cycling stability of the anode. However, the battery seems like a

black box, as the microscopic process of the reaction can hardly be investigated. To further study the electrode process during cycling, the reaction rate and Na⁺ distribution in the whole volume of electrode were simulated by the finite element method in COMSOL Multiphysics. Simulation of the cell geometry for the hybrid anode is shown in Fig. S10 (online). It is commonly recognized that Na will be deposited at positions where sufficient Na⁺ ions and electrons are both provided (i.e., ion/electron interface) during the plating process [38]. For the bare Na electrode (Fig. 4a, c), the Na plating is concentrated on the planar surface of Na- metal due to the poor ionic conductivity of solid Na metal. By contrast, the Na ions can be transferred into the depth of the electrode along the NZSP skeleton (Fig. 4d), where more ion/electron interfaces are available for fast redox reactions (Fig. 4b), and the reaction processcan be seen in detail in Movie S1. In addition, under the same voltage of 0.1 V, the time required to reach steady state is much shorter and the steady state current is larger (Fig. 4e, f), which confirms that more Na⁺ is available for the reaction, and the electrochemical reaction inBH-Na is more easily to occur. This is own to mixed electron/ion transport pathways and two-phase boundaries throughout the electrode, which is consistent with the above EIS and Tafel results.

To better understand the electrochemical stability of the BH-Na electrode, the morphological changes in both electrodes before and after cycling were investigated as shown in Fig. 5. The surface of the bare Na-metal changes from the initial flat state to a rough and porous structure, with rod-like and moss-like dendrites after cycling (Fig. 5a, b). In contrast, there is no obvious change in the morphology of the BH-Na electrode, where a compact configuration is well maintained (Fig. 5c, d), indicating that such hybrid design effectively inhibits the evolution of dendrites. A direct comparison of the glass fiber separators of the disassembled batteries also displays the difference (Fig. S11 online). Black-gray contaminants can be observed in the glass fiber separator of the cell with the bare Na electrode after cycling.

This may be dendrites growing from the surface of bare Na-metal to the interior of the

separator, which is a hidden danger of battery short-circuiting. Conversely, the separator in the cell with the BH-Na electrode exhibits a clean surface after cycling, indicating uniform plating/stripping behavior on the BH-Na electrode.

To consolidate our conclusion, asymmetric batteries with one BH-Na electrode and one Na-metal electrode were assembled to study the morphology evolution of the BH-Na electrode under deep charge and discharge of 10 mAh cm⁻² (~27% capacity of electrode). After stripping 10 mAh cm⁻² Na from the BH-Na anode (Fig. 5e, f), submicron and nanosized pores are observed in the electrode, which were initially occupied by Na, and the structure of the NZSP remains intact. Followed by the Na plating of 10 mAh cm⁻² (Fig. 5g), it is observed that Na has been refilled back into the NZSP network without uneven deposition of Na and the formation of dendrites. These results indicate that the BH-Na anode can effectively inhibitthe formation of dendrites and adjust the plating and stripping behavior of Na into the depthof electrode, which coincides with the analysis of the voltage curve in the symmetrical cells.

Full cells with Na₃V₂(PO₄)₃/C (NVP) cathode were assembled to investigate the practicality of the BH-Na anode. The NVP/Na cell was also assembled for comparison. As shown in Fig. 6a, the NVP/BH-Na cell delivers a capacity of 102 mAh g⁻¹ with small capacity decay of 0.012% per cycle at 5 C (1 C = 117 mA g⁻¹). Instead, the NVP/Na cell exhibits a lower capacity of 93 mAh g⁻¹, and its Coulombic efficiency drops rapidly after 1200 cycles, which indicates the failure of the cell. According to the galvanostatic charge/discharge curves of the NVP/BH-Na cell (Fig. 6b), no obvious changes in capacity and polarization over 1 to 200 cycles are observed, indicating excellent cycling stability of the cell. Moreover, derived from the fast ion transport characteristics of the BH-Na anode, the full cell delivers much smaller polarization than the NVP/Na cell (112 mV vs. 440 mV in the 200th cycle, Fig. 6c). The largepolarization in the latter cell is mainly related to the large overpotential of the bare Na anode, which is the primary culprit for its lower capacity as the results on symmetrical cells (Fig. 2).

4. Conclusion

In summary, focusing on improving Na-ion conduction within the whole electrode volume of Na-metal-based anode, a bulk hybrid anode was fabricated through incorporating NaSICON-type solid electrolyte into bulk Na by a facile and scalable melt infusion method. In our proposed hybrid anode design, with the fast Na⁺ conduction of NZSP network and compact configuration of electrode, the reaction area for the plating/stripping of Na is enlarged to the whole electrode volume rather than concentrated on the surface of the electrode. The ceramic electrolyte skeleton greatly inhibits large volume changes and uneven plating/stripping behavior on the surface of the electrode. In addition, the enhancement of mechanical strength of the electrode introduced by NZSP particles can also inhibit dendrite growth. Correspondingly, symmetric and full cells with the BH-Na anode exhibit low voltage hysteresis and stable cycling in carbonate electrolyte.

Conflict of interest

The authors declare that they have no conflict of interest.

Acknowledgments

This work was supported by the National Natural Science Foundation of China (51722105), Zhejiang Provincial Natural Science Foundation of China (LR18B030001), and Ten Thousand Talent Program of Zhejiang Province.

Author contributions

Yinzhu Jiang conceived this idea and directed this project. Keshuang Cao performed the experiments and contributed to data interpretation. Qianli Ma helped in preparing the samples and assembling the cells. Yinzhu Jiang and Keshuang Cao co-wrote the paper. Qianli Ma, Frank Tietz, Ben Bin Xu and Mi Yan discussed the results and commented on the manuscript.

References

- [1] Lu J, Chen Z, Pan F, et al. High-performance anode materials for rechargeable lithium-ion batteries. Electrochem Energ Rev 2018;1:35-53.
- [2] Li L, Zheng Y, Zhang S, et al. Recent progress on sodium ion batteries: potential high-performance anodes. Energy Environ Sci 2018;11:2310-40.
- [3] Yang H, Cui W, Han Y, et al. Porous nanocomposite derived from Zn, Ni-bimetallic metal-organic framework as an anode material for lithium-ion batteries. Chin Chem Lett 2018;29:842-4.
- [4] Grosjean C, Miranda PH, Perrin M, et al. Assessment of world lithium resources and consequences of their geographic distribution on the expected development of the electric vehicle industry. Renew Sust Energ Rev 2012;16:1735-44.
- [5] Hwang JY, Myung ST, Sun YK. Sodium-ion batteries: present and future. Chem Soc Rev 2017;46:3529-614.
- [6] Xu G, Amine R, Abouimrane A, et al. Challenges in developing electrodes, electrolytes, and diagnostics tools to understand and advance sodium-ion batteries. Adv Energy Mater 2018;8:1702403.
- [7] Xu J, Gu E, Zhang Z, et al. Fabrication of porous Na₃V₂(PO₄)₃/reduced graphene oxide hollow spheres with enhanced sodium storage performance. J Colloid Interface Sci 2020;567:84-91.
- [8] Ge X, Liu S, Qiao M, et al. Enabling superior electrochemical properties for highly efficient potassium storage by impregnating ultrafine Sb nanocrystals within nanochannel containing carbon nanofibers. Angew Chem Int Ed 2019;131:14720-5.
- [9] Che H, Chen S, Xie Y, et al. Electrolyte design strategies and research progress for room-temperature sodium-ion batteries. Energy Environ Sci 2017;10:1075-101.
- [10] Huang Y, Zhao L, Li L, et al. Electrolytes and electrolyte/electrode interfaces in sodium-ion batteries: From scientific research to practical application. Adv Mater 2019;0:1808393.
- [11] Cheng Z, Mao Y, Dong Q, et al. Fluoroethylene carbonate as an additive for sodium-ion batteries: Effect on the sodium cathode. Acta Phys Chim Sin 2019;35:868-75.
- [12] Li M, Feng N, Liu M, et al. Hierarchically porous carbon/red phosphorus composite for high-capacity sodium-ion battery anode. Sci Bull 2018;63:982-9.
- [13] Stevens DA, Dahn JR. The mechanisms of lithium and sodium insertion in carbon materials. J Electrochem Soc 2001;148:803-11.
- [14] Shen Y, Li Y, Deng S, et al. TiC/C core/shell nanowires arrays as advanced anode of sodium ion batteries. Chin Chem Lett 2020;31:846-50.

- [15] Nayak PK, Yang L, Brehm W, et al. From lithium-ion to sodium-ion batteries: Advantages, challenges, and surprises. Angew Chem Int Ed 2018;57:102-20.
- [16] Lu X, Luo J, Matios E, et al. Enabling high-performance sodium metal anodes via a sodiophilic structure constructed by hierarchical Sb₂MoO₆ microspheres. Nano Energy 2020;69:104446.
- [17] Sun B, Xiong P, Maitra U, et al. Design strategies to enable the efficient use of sodiummetal anodes in high-energy batteries. Adv Mater 2019;0:1903891.
- [18] Lee B, Paek E, Mitlin D, et al. Sodium metal anodes: Emerging solutions to dendrite growth. Chem Rev 2019;119:5416-60.
- [19] Zhao Y, Adair KR, Sun X. Recent developments and insights into the understanding of Na metal anodes for Na-metal batteries. Energy Environ Sci 2018;11:2673-95.
- [20] Wang G, Xiong X, Xie D, et al. A scalable approach for dendrite-free alkali metal anodes via room-temperature facile surface fluorination. ACS Appl Mater Interfaces 2019;11:4962-8.
- [21] Choudhury S, Wei S, Ozhabes Y, et al. Designing solid-liquid interphases for sodium batteries. Nat Commun 2017;8:898.
- [22] Zhao Y, Goncharova LV, Zhang Q, et al. Inorganic-organic coating via molecular layer deposition enables long life sodium metal anode. Nano Lett 2017;17:5653-9.
- [23] Wang C, Wang H, Matios E, et al. A chemically engineered porous copper matrix with cylindrical core—shell skeleton as a stable host for metallic sodium anodes. Adv Funct Mater 2018;28:1802282.
- [24] Sun J, Guo C, Cai Y, et al. Dendrite-free and long-life Na metal anode achieved by 3Dporous Cu. Electrochim Acta 2019;309:18-24.
- [25] Hu X, Joo PH, Wang H, et al. Nip the sodium dendrites in the bud on planar doped graphene in liquid/gel electrolytes. Adv Funct Mater 2019;29:1807974.
- [26] Wang H, Matios E, Wang C, et al. Tin nanoparticles embedded in a carbon bufferlayer as preferential nucleation sites for stable sodium metal anodes. J Mater Chem A 2019;7:23747-55.
- [27] Wang A, Hu X, Tang H, et al. Processable and moldable sodium-metal anodes. AngewChem Int Ed 2017;56:11921-6.
- [28] Luo J, Wang C, Wang H, et al. Pillared Mxene with ultralarge interlayer spacing as a stable matrix for high performance sodium metal anodes. Adv Funct Mater 2019;29:1805946.

- [29] Lin D, Zhao J, Sun J, et al. Three-dimensional stable lithium metal anode with nanoscale lithium islands embedded in ionically conductive solid matrix. Proc Natl Acad Sci USA 2017;114:4613-8.
- [30] Ma Q, Tsai CL, Wei X, et al. Room temperature demonstration of a sodium superionic conductor with grain conductivity in excess of 0.01 S cm⁻¹ and its primary applications in symmetric battery cells. J Mater Chem A 2019;7:7766-76.
- [31] Li W, Yao Z, Zhong Y, et al. Enhancement of the advanced na storage performance of Na₃V₂(PO₄)₃ in a symmetric sodium full cell via a dual strategy design. J Mater Chem A 2019;7:10231-8.
- [32] Zhang W, Fan L, Tong Z, et al. Stable Li-metal deposition via a 3D nanodiamond matrix with ultrahigh young's modulus. Small Methods 2019;0:1900325.
- [33] Seh ZW, Sun J, Sun Y, et al. A highly reversible room-temperature sodium metal anode. ACS Cent Sci 2015;1:449-55.
- [34] Zheng X, Fu H, Hu C, et al. Toward a stable sodium metal anode in carbonate electrolyte: a compact, inorganic alloy interface. J Phys Chem Lett 2019;10:707-14.
- [35] Park MS, Ma SB, Lee DJ, et al. A highly reversible lithium metal anode. Sci Rep 2014;4:3815.
- [36] Wood KN, Kazyak E, Chadwick AF, et al. Dendrites and pits: Untangling the complex behavior of lithium metal anodes through operando video microscopy. ACS Cent Sci 2016;2:790-801.
- [37] Barbir F. Fuel cell electrochemistry. In: Barbir F, editors. PEM fuel cells. Burlington: Academic Press; 2005. 33-72.
- [38] Zhou F, Li Z, Lu Y, et al. Diatomite derived hierarchical hybrid anode for high performance all-solid-state lithium metal batteries. Nat Commun 2019;10:2482.



Keshuang Cao received his B.E. degree in Materials Science and Engineering from Zhejiang University of Technology in 2018. He is currently pursuing his Ph.D. degree at Zhejiang University. His current research interests focus on alkali metal anodes for advanced rechargeable alkali metal batteries.



Qianli Ma obtained B.S. and Ph.D. degrees at the University of Science and Technology of China, majored in Materials Science. From 2007 to present, he is working in Forschungszentrum Jülich, IEK-1, Germany, first as post-doc, then as senior scientist, and now as tenure scientist. Hespecializes in development of non-metallic inorganic materials. He has detailed researching experiences on the relationships between processing, microstructure and properties, and is especially familiar with R & D of solid-state batteries and fuel cells.



Yinzhu Jiang is a full professor at School of Materials Science and Engineering in Zhejiang University, China. He received his Ph.D. degree in Department of Materials Science and

Engineering from University of Science and Technology of China in 2007. He worked as post-doctoral researcher in Heriot-Watt University, UK from 2007 to 2008 and an Alexander von Humboldt Fellow in Bielefeld University, Germany from 2008 to 2010. His research interests focus mainly on energy-related materials and electrochemistry, including rechargeable batteries, metal anodes and solid electrolytes.

Fig. 1. (Color online) Schematic and characterization of BH-Na. (a) Schematic diagram of fabrication process of the BH-Na anode. (b) Schematic of Na⁺ transfer in bare Na and BH-Na anode. (c) SEM images, (d) EDS mapping and (e) XRD pattern of SnO₂@NZSP. SEM images of pristine BH-Na anode (f) and after stripping all the sodium (g). (h) Hardness measurement results of the bare Na and BH-Na anode with a Shore A durometer.

Fig. 2. (Color online) Electrochemical performance of the BH-Na anode. (a) Voltage profiles of symmetric cells with the BH-Na anode and bare Na anode at current density of 1 mA cm⁻² with fixed capacity of 1 mAh cm⁻². (b) Impedance spectra and (c) Tafel plot of bare Na anode and BH-Na anode after 10 cycles.

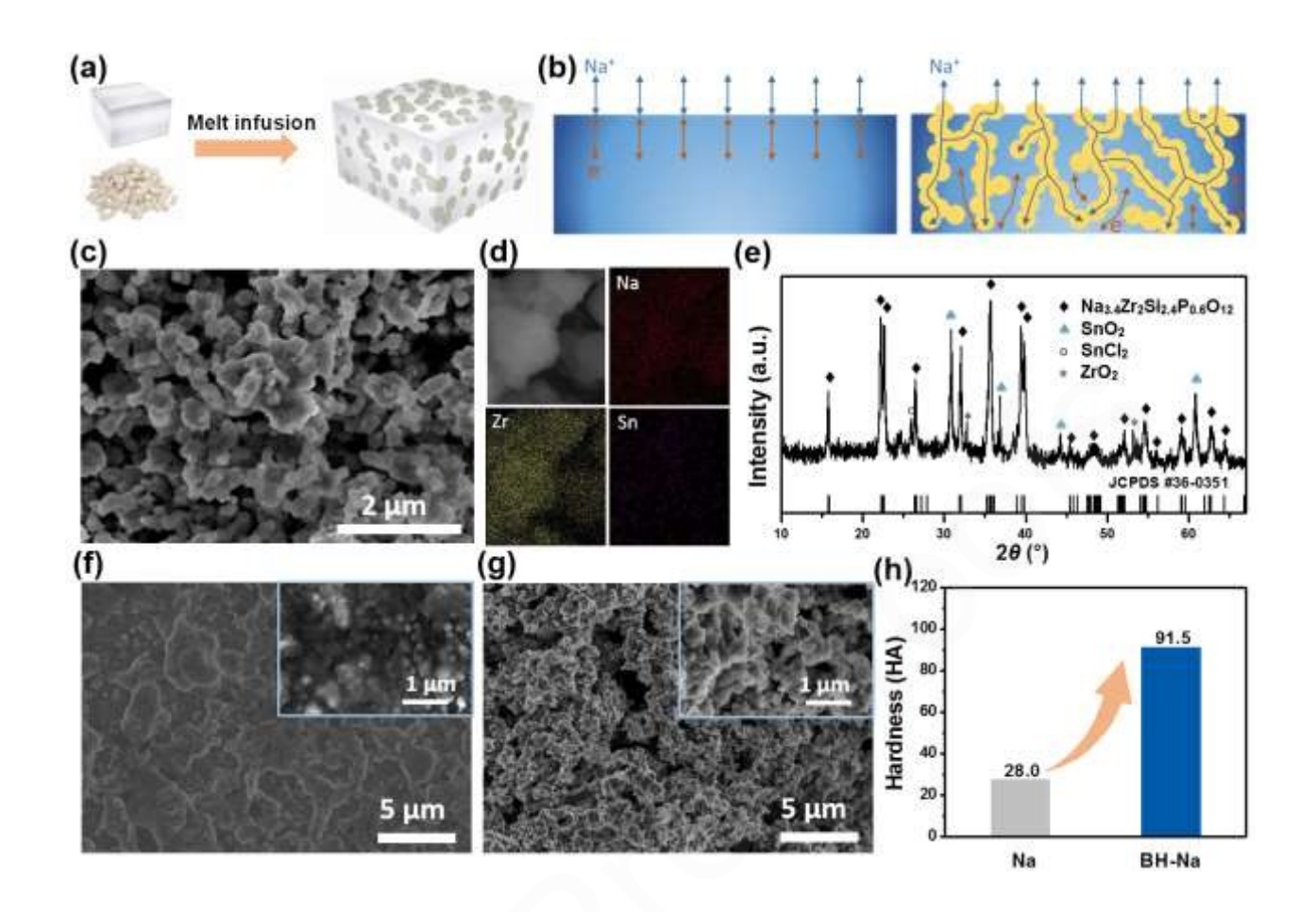
Fig. 3. (Color online) Galvanostatic cycling stability of the BH-Na anode and bare Na anode in symmetric cells at (a) 1 mA cm⁻² for 5 mAh cm⁻², (b) 3 mA cm⁻² for 3 mAh cm⁻² and (c) at a fixed capacity of 1 mAh cm⁻² along with rate current densities of 1, 2, 5 and 8 mA cm⁻² and back to 1 mA cm⁻².

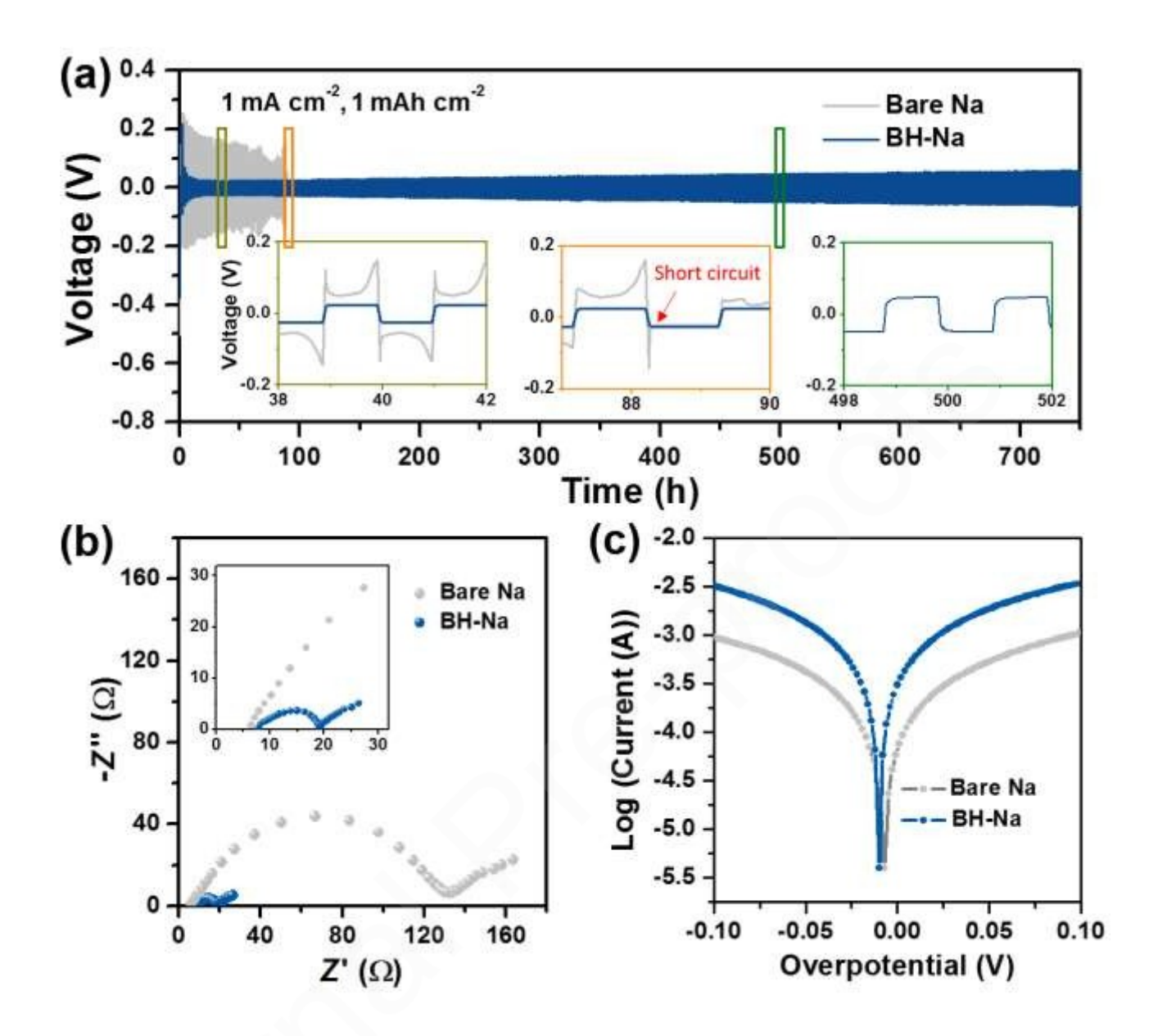
Fig. 4. (Color online) COMSOL multiphysics modeling of the BH-Na anode geometry during Na plating. Simulation results of reaction rate distributions for the bare Na anode (a) and the BH-Na anode (b). Simulation of the Na-ion distributions in the bare Na anode (c) and the BH-Na anode (d). These are the results under steady state. The simulated curves of current varying with simulation time in bare Na (e) and BH-Na (f).

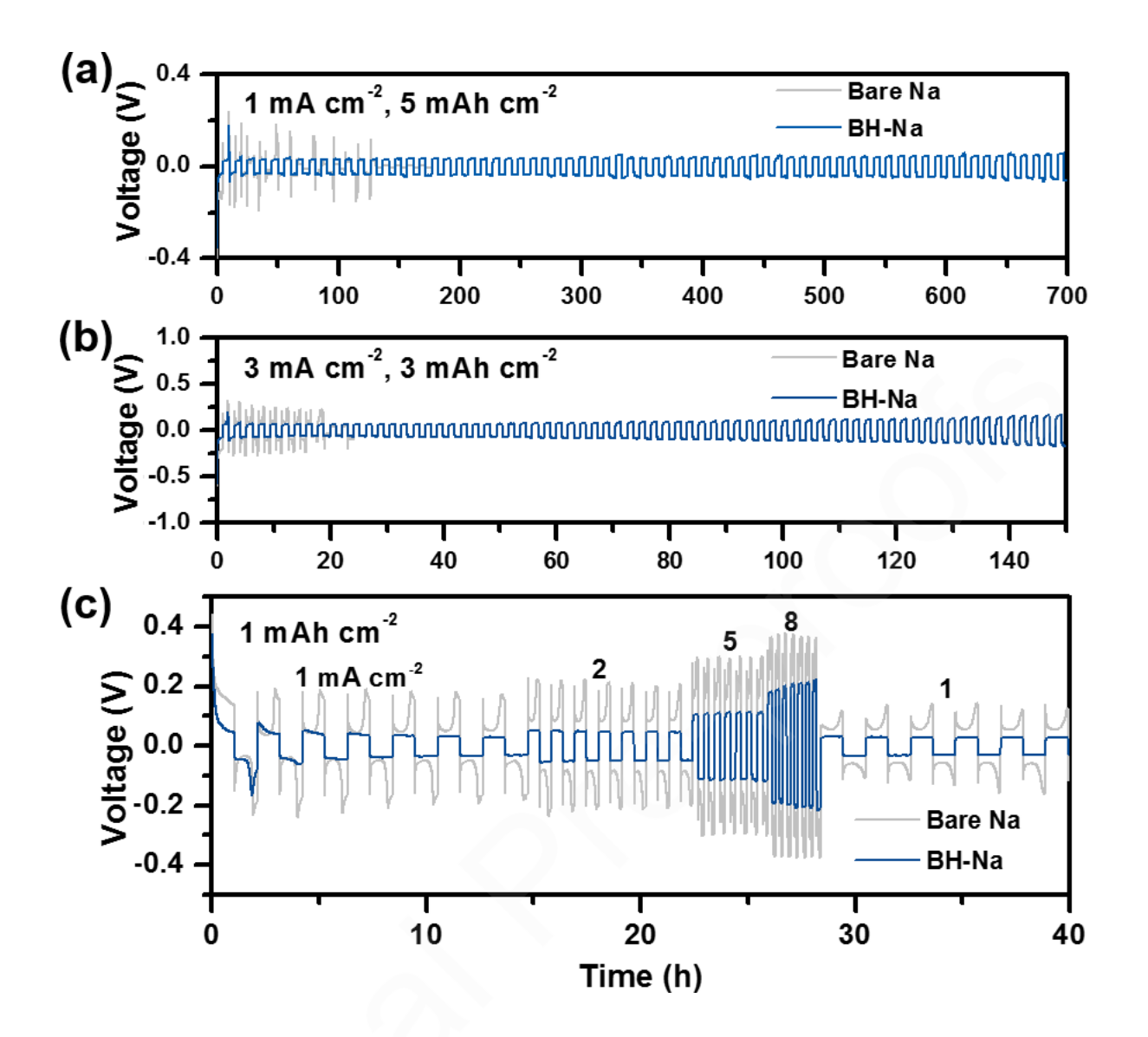
Fig. 5. (Color online) Morphology characterization of electrodes before and after cycling. SEM images of Na anode (a) and BH-Na anode (c) before cycling as well as Na anode (b) and BH-Na

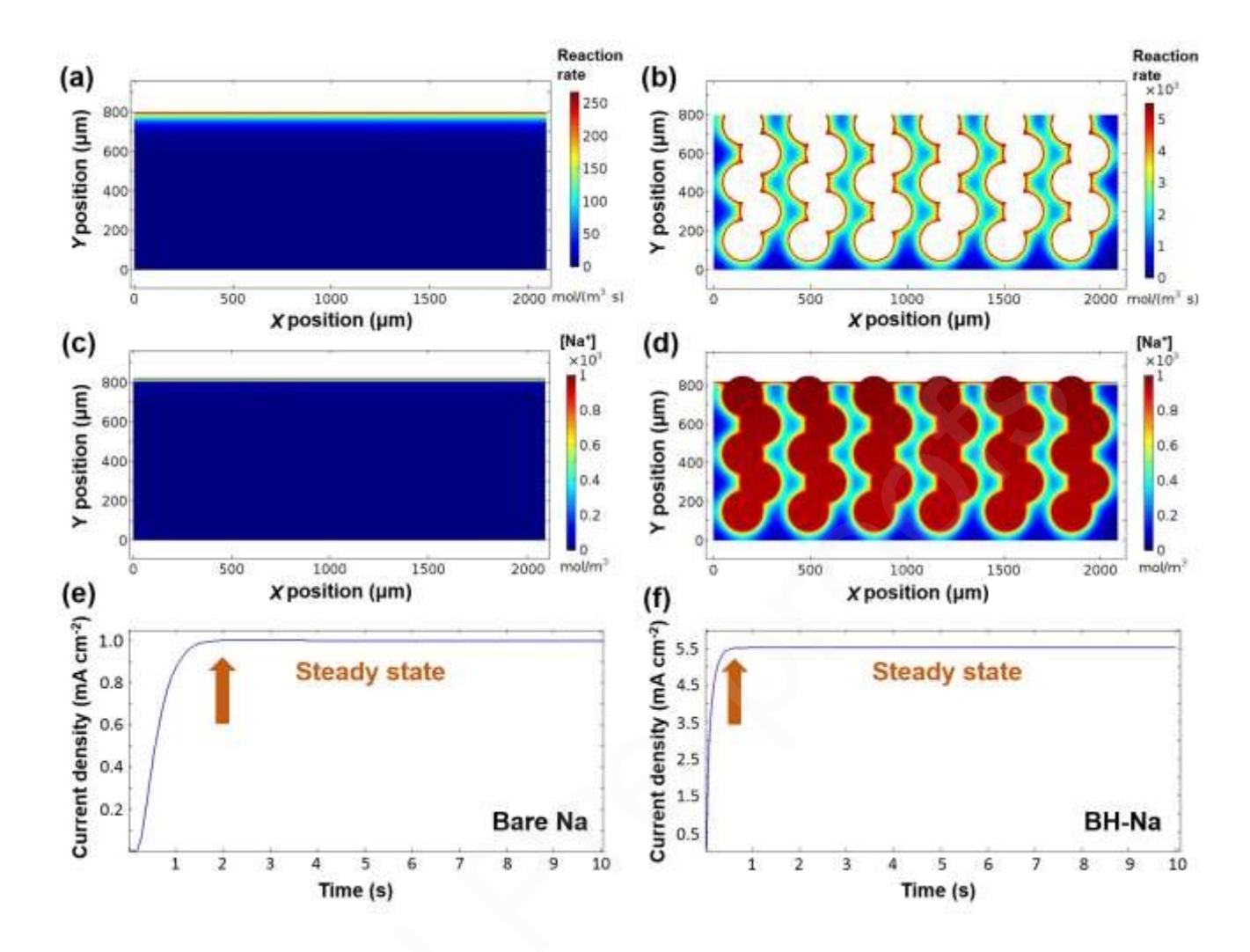
anode (d) after 20 cycles at 1 mA cm⁻², 1 mAh cm⁻². Enlarged SEM images of pristine BH-Na anode (e), after stripping 10 mAh cm⁻² (f) and after subsequent plating 10 mAh cm⁻² of Na (g).

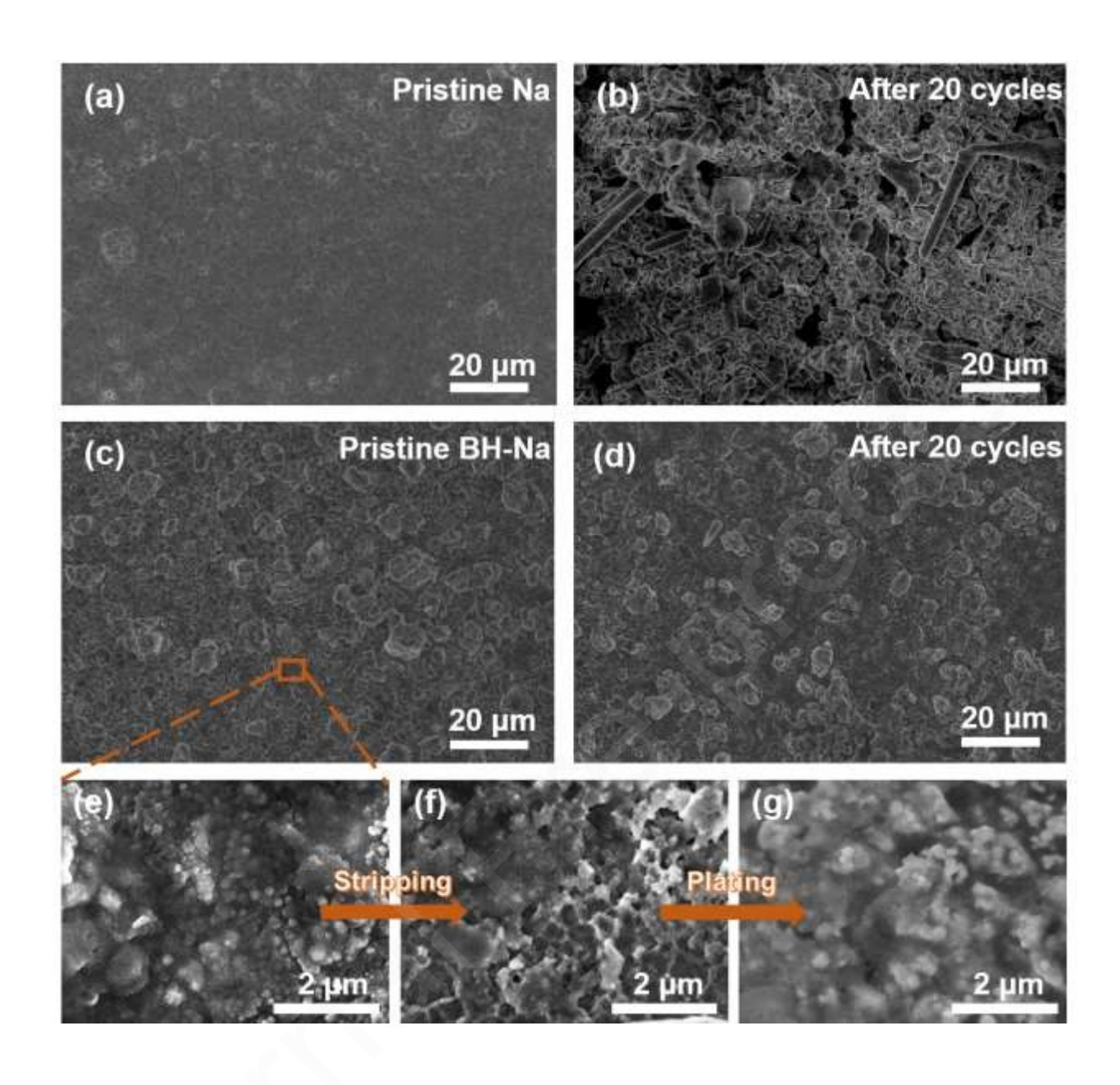
Fig. 6. (Color online) The electrochemical performance of full cells with bare Na anode and BH-Na anode. (a) Cycling performance at 5 C, (b) galvanostatic charge-discharge curves of full cell with BH-Na anode, (c) charge-discharge curves of 200th cycle of full cells with bare Na anode and BH-Na anode.

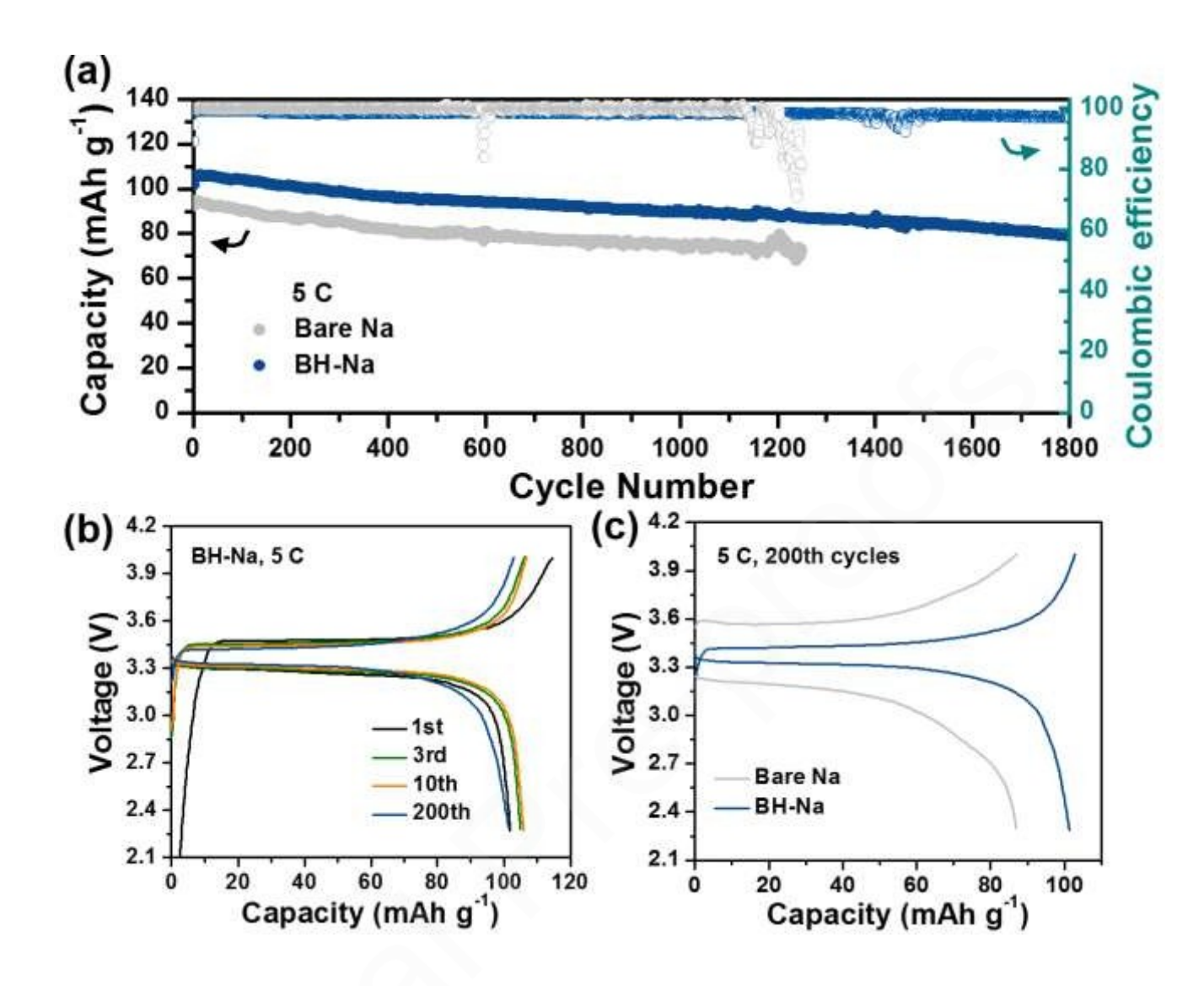


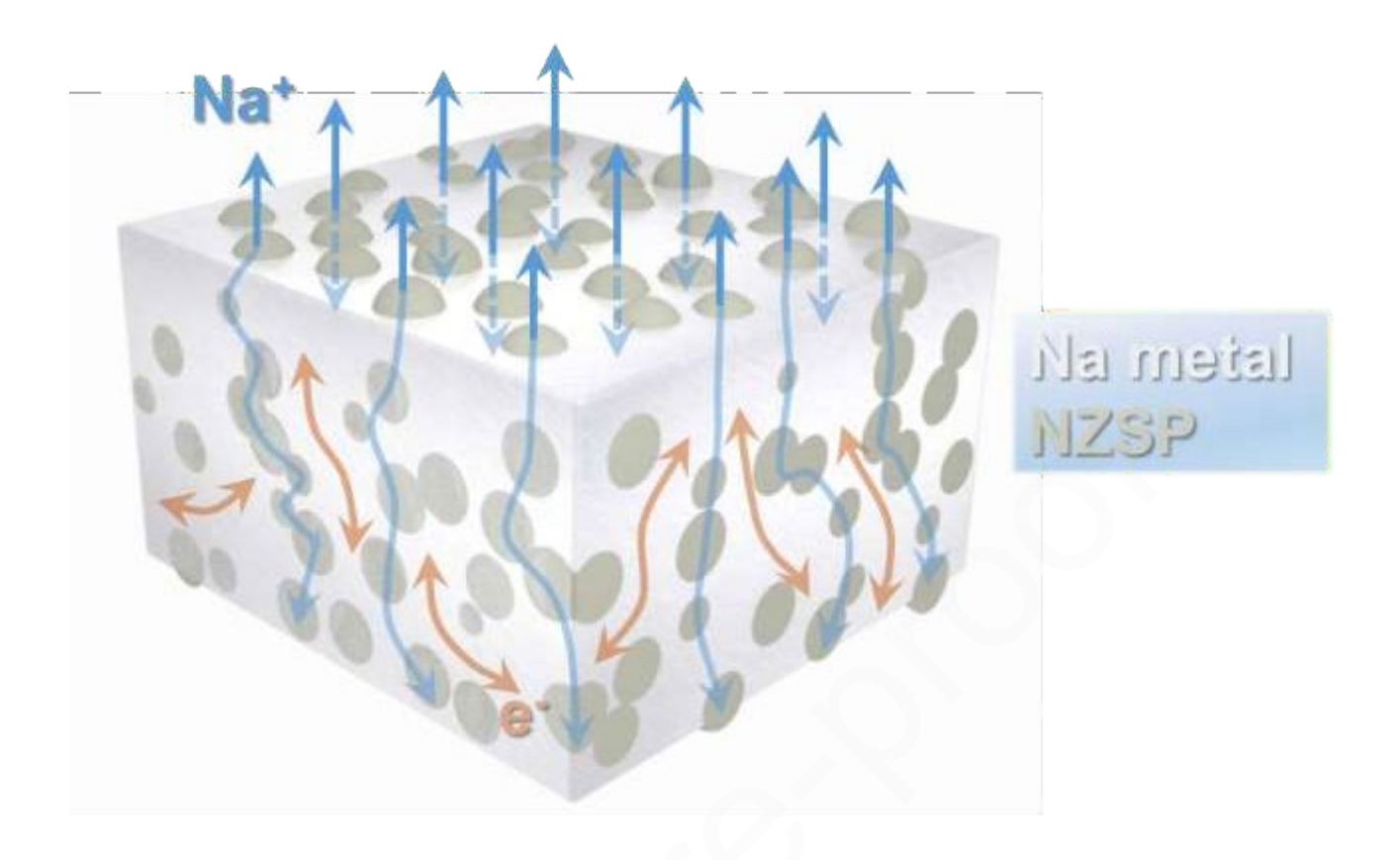












Bulk hybrid Na-metal anode